Supercond. Sci. Technol. **21** (2008) 095008 (11pp) doi:10.1088/0953-2048/21/9/095008

Evidence for two distinct scales of current flow in polycrystalline Sm and Nd iron oxypnictides

A Yamamoto[1], A A Polyanskii[1], J Jiang[1], F Kametani[1], C Tarantini[1], F Hunte[1], J Jaroszynski[1], E E Hellstrom[1], P J Lee[1], A Gurevich[1], D C Larbalestier[1], Z A Ren[2], J Yang[2], X L Dong[2], W Lu[2] and Z X Zhao[2]

[1] National High Magnetic Field Laboratory, Florida State University, Tallahassee, FL 32310, USA
[2] National Laboratory for Superconductivity, Institute of Physics and Beijing National Laboratory for Condensed Matter Physics, Chinese Academy of Sciences, PO Box 603, Beijing 100190, People's Republic of China

E-mail: yamamoto@asc.magnet.fsu.edu and larbalestier@asc.magnet.fsu.edu

Received 4 June 2008, in final form 15 June 2008
Published 4 July 2008
Online at stacks.iop.org/SUST/21/095008

Abstract
Early studies have found quasi-reversible magnetization curves in polycrystalline bulk rare-earth iron oxypnictides that suggest either widely spread obstacles to intergranular current or very weak vortex pinning. In the present study of polycrystalline samarium and neodymium iron oxypnictide samples made by high pressure synthesis, the hysteretic magnetization is significantly enhanced. Magneto-optical imaging and study of the field dependence of the remanent magnetization as a function of particle size both show that global currents over the whole sample do exist but that the intergranular and intragranular current densities have distinctively different temperature dependences and differ in magnitude by about 1000. If the highest current density loops lie only within grains, their magnitude is $\sim 5 \times 10^6$ A cm^{-2} at 5 K and self-field. Whole sample current densities, though two orders of magnitude lower at 1000–10 000 A cm^{-2}, are some two orders of magnitude higher than in random polycrystalline cuprates. We cannot yet be certain whether this large difference in global and intragrain current density is intrinsic to the oxypnictides or due to extrinsic barriers to current flow, because the samples contain a significant second phase, some of which wets the grain boundaries and may cause a superconducting–normal–superconducting proximity effect in the whole sample critical current.

(Some figures in this article are in colour only in the electronic version)

1. Introduction

The recent discovery of superconductivity in the $LaFeAsO_{1-x}F_x$ compound [1] has stimulated a rapid exploration of superconductivity in the rare-earth iron oxypnictides [2–14]. It has now been established that the iron oxypnictides can be superconducting when doped to $x \sim 0.05$–0.2 and that they can have transition temperature T_c above 40 K when La is replaced by Ce [5] and above 50 K by Pr, Nd, Sm and Gd [7–11]. In a recent paper [12] we addressed the issue of electromagnetic granularity in polycrystalline La iron oxypnictides, finding an asymmetric $M(H)$ loop that indicated an irreversible moment due to hysteretic bulk currents that was almost as small as the reversible magnetization of the superconducting state. In that case we were not able to distinguish definitively between a state where the intragrain pinning was very weak, leading to very low intragrain current densities or to the state where currents were largely confined to the intragrain regions and might have been rather high. Based on the rather high upper critical field $B_{c2}(0)$ values of

63–65 T observed by Hunte *et al* [6] on the same sample and the nanoscale coherence length ξ ($\xi^{ab}(0) = 5$ nm, $\xi^{c}(0) = 1.2$ nm), we would expect strong vortex pinning even from naturally occurring atomic-scale defects. By analogy to randomly oriented polycrystalline cuprates, which also show small hysteretic current loops and large intragrain current densities of 10^5–10^6 A cm^{-2} at 4 K [15, 16], we proposed [12] that electromagnetic granularity was likely to be characteristic of polycrystalline oxypnictides too. By granularity we mean that two distinct scales of current flow would exist. The intragrain current would be dominated by vortex pinning, while the global current would be limited by connections across grain boundaries, some of which might be superconducting (S), some normal (N) or some even insulating (I). In the case of SNS or SIS connections, we would expect clear evidence that the global current density would be lower than the current circulating on scales where the whole path was superconducting. Evidence for electromagnetically granular behavior was indeed also presented in two subsequent studies of a Sm oxypnictide (Senatore *et al* [13]) and a Nd oxypnictide (Prozorov *et al* [14]), the latter of which also presented magneto-optical images of confined current flow within intragranular regions. In the present study, we extend our initial examination of the length scales of current flow in La oxypnictide by combining magneto-optical imaging, remanent magnetic field analysis and powdering of the sample to conclusively demonstrate the presence of two distinctly different length scales of current flow in our dense Nd and Sm oxypnictides and to show that the temperature dependence of the inter and intragranular current densities are quite different and that their ratio is strongly dependent on temperature.

2. Experimental details

The polycrystalline $SmFeAsO_{0.85}$ and $NdFeAsO_{0.94}F_{0.06}$ bulk samples were synthesized by solid state reaction under a high pressure [8, 10]. SmAs (or NdAs) pre-sintered powder and Fe, Fe_2O_3, and FeF_2 powders were mixed together according to the nominal stoichiometric ratio then ground thoroughly and pressed into small pellets. The pellets were sealed in boron nitride crucibles and sintered in a high pressure synthesis apparatus under a pressure of 6 GPa at 1250 °C for 2 h.

Microstructural observations were performed using a field emission scanning electron microscope (Carl Zeiss 1540 ESB and XB) and a laser scanning confocal microscope (Olympus OLS3100). Resistivity measurements were performed by the conventional four-point-probe method using a Quantum Design PPMS. Magnetization of the samples was measured by a SQUID magnetometer (Quantum Design: MPMS-XL5s) and a 14 T vibrating sample magnetometer (Oxford) with field parallel to the broad face. Magneto-optical imaging with a 5 μm thick Bi-doped iron-garnet indicator film placed directly onto the sample surface was used to image the normal field component B_z produced by magnetization currents induced by solenoidal fields of up to 0.12 T applied perpendicular to the imaged surface [17, 18].

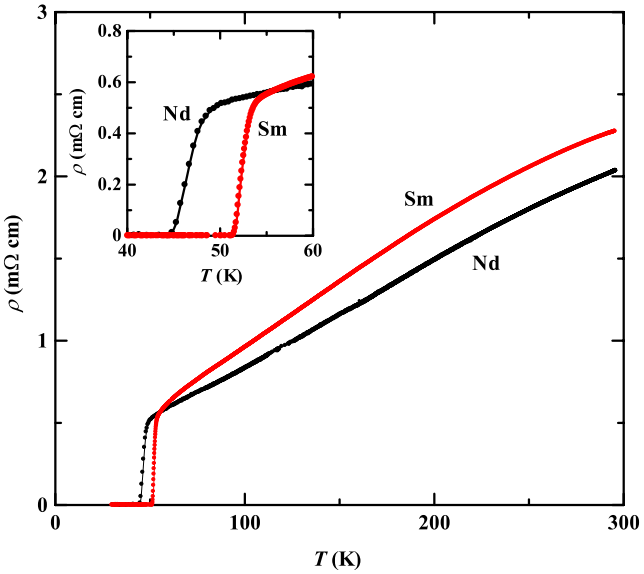

Figure 1. Temperature dependence of resistivity for the $SmFeAsO_{0.85}$ and $NdFeAsO_{0.94}F_{0.06}$ bulk samples. Inset shows resistivity near T_c.

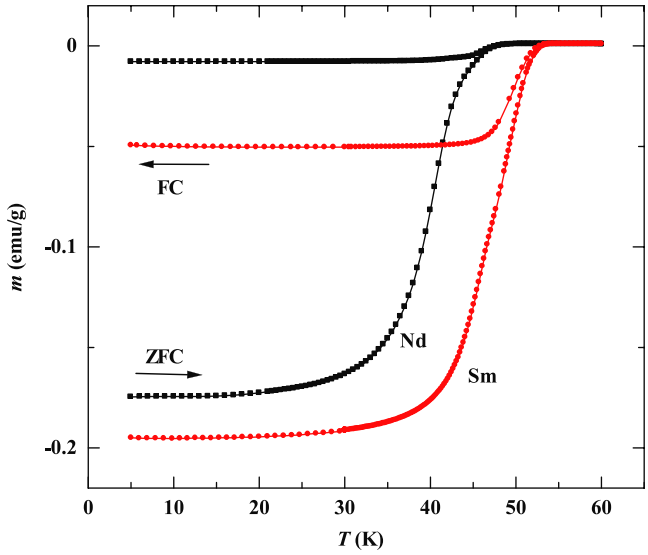

Figure 2. Temperature dependence of magnetization under zero-field-cooling (ZFC) and field-cooling (FC) conditions in an external field of 1 mT for bulk $SmFeAsO_{0.85}$ and $NdFeAsO_{0.94}F_{0.06}$.

3. Results

The temperature dependences of resistivity for the $SmFeAsO_{0.85}$ and $NdFeAsO_{0.94}F_{0.06}$ bulk samples are shown in figure 1. Resistivity began to drop at 57 and 51 K and vanished below 51 and 44 K for the Sm and Nd samples, respectively. The calculated resistivities at 300 K for the Sm and Nd samples were 2.3 and 2.0 mΩ cm and the $RRR = \rho(300\text{ K})/\rho(60\text{ K})$ were 3.7 and 3.4, respectively. By contrast the RRR value of 17 was observed for the earlier studied $LaFeAsO_{0.89}F_{0.11}$ bulk sample [4, 12], which might suggest that the Sm and Nd samples are less strongly doped and that the actual doping state may not be well represented by the nominal composition.

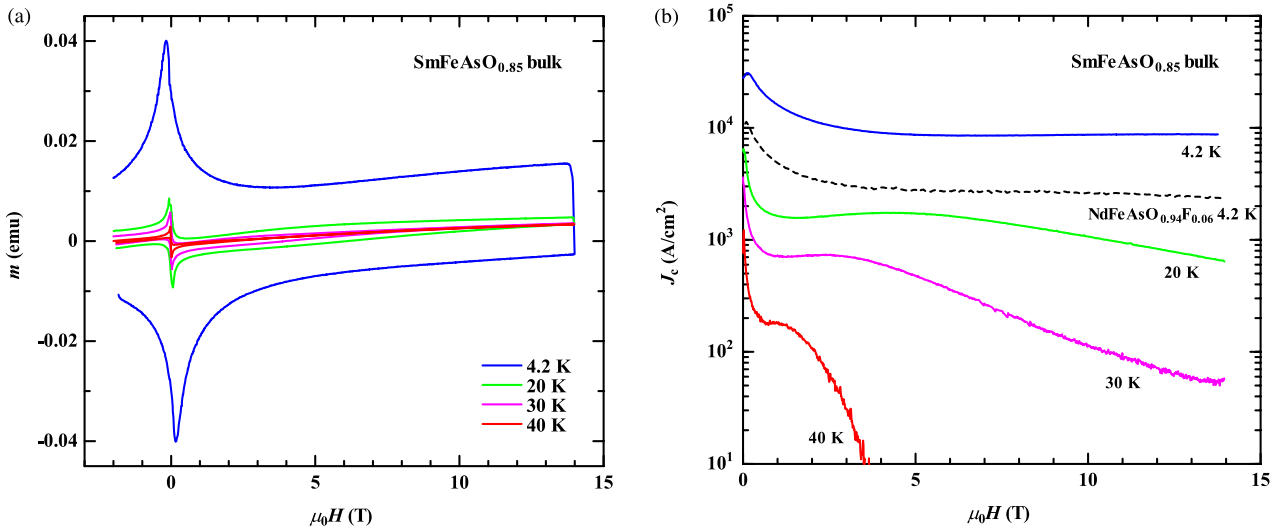

Figure 3. Magnetization hysteresis loops (a) and magnetic field dependence of J_c (b) at 4.2, 20, 30 and 40 K for $SmFeAsO_{0.85}$ bulk. J_c data for $NdFeAsO_{0.94}F_{0.06}$ bulk at 4.2 K (dashed line) is also shown for comparison.

Figure 2 shows the temperature dependences of magnetization in zero-field-cooled (ZFC) and field-cooled (FC) states under an external field of 1 mT. Onset magnetic T_c values were found to be 54 K for the Sm sample and 49 K for the Nd sample. Compared to the $LaFeAsO_{0.89}F_{0.11}$ sample [12] and other reported samples [13, 14], superconducting transitions are rather sharp ($\Delta T_c \sim 10$ K), indicative of bulk scale shielding currents flowing in both samples, even close to T_c. Within the uncertainty limits produced by the demagnetization fields of these imperfectly shaped samples, we conclude that the shielded volumes were 100%.

Figure 3(a) shows magnetic hysteresis loops at 4.2, 20, 30 and 40 K obtained by VSM for the $SmFeAsO_{0.85}$ bulk sample. So far very small hysteresis loops were reported for polycrystalline iron oxypnictides [12, 13]. However, this Sm sample shows quite large hysteresis loops, which implies either strong flux pinning and/or good intergranular coupling. Slightly smaller hysteresis loop widths were observed in the Nd sample. Similar to the previously studied $LaFeAsO_{0.89}F_{0.11}$ sample [12], a paramagnetic background was observed in all curves taken below T_c, which can be well fit by a Langevin expression [19].

Figure 3(b) shows the magnetic field dependence of the critical current density J_c derived from the hysteresis loop width using the extended Bean model $J_c = 20\Delta m/Va(1 - a/3b)$ for the Sm bulk sample taking the full sample dimensions of $2 \times 1 \times 0.6$ mm^3. This expression yields a J_c of 100 00–300 00 A cm^{-2} at 4.2 K, which is nearly independent of field over the range of 4–14 T. J_c for the Nd bulk sample is lower, as is shown in figure 3(b). Broad maximum in $J_c(B)$ was observed at 20, 30 and 40 K, a result also noted in [13]. Since the contribution of currents circulating on smaller length scales to the hysteresis loop is large, as discussed later, the critical current density shown in figure 3(b) is likely to be overestimated, since our later, size-dependent studies allow us to deduce that the contribution of global currents to the hysteretic magnetization is less than that produced by the locally circulating currents. However, these J_c values are distinctly better than randomly oriented polycrystalline cuprates, which are typically ∼100 A cm^{-2} [16]. It is also important to note that the relatively large hysteresis loop and finite J_c values observed in the Sm and Nd samples are in strong contrast to the almost reversible magnetization observed in the $LaFeAsO_{0.89}F_{0.11}$ sample where bulk flux shielding was not visible in magneto-optical images.

Figure 4(a) shows a whole sample image of the $SmFeAsO_{0.85}$ bulk obtained by scanning electron microscopy. The bulk sample has a relative density of ∼90%. High magnification images of the polished surface of the $SmFeAsO_{0.85}$ revealed plate-like grains of the superconducting phase with a size of ∼10 μm, as shown in figure 4(b). Atomic number sensitive back-scattered electron (BSE) imaging also revealed that the sample contains multiple impurity phases, with the two most prominent phases, as shown in figure 4(b), identified by EDS as Sm_2O_3 (white contrast) and Fe–As glassy phase (dark contrast). It does appear that the microstructure is homogeneous on the macroscale, although the Nd bulk sample showed macroscale inhomogeneity on a scale of several hundred micrometers (see figure 8(a)). The larger fraction of impurity phases in the Nd bulk is consistent with its lower J_c compared to that of the Sm bulk.

Figure 4(c) shows a laser scanning microscope image of the crushed pieces of $SmFeAsO_{0.85}$ with particle size of ∼500 μm, while figure 4(d) shows a scanning electron microscope image of the ground powder. Most of the particles are less than 100 μm in size, having an average size of 20–50 μm. Higher magnification SEM images revealed that each particle still contains several to several tens of grains, even after fine grinding.

In order to make a more explicit test of the scale over which currents flow, we made remanent magnetization analysis on polycrystalline samples of different size. Both intact bulk samples were exposed to many cycles of ever increasing magnetic field H_a, followed by removal of the field and

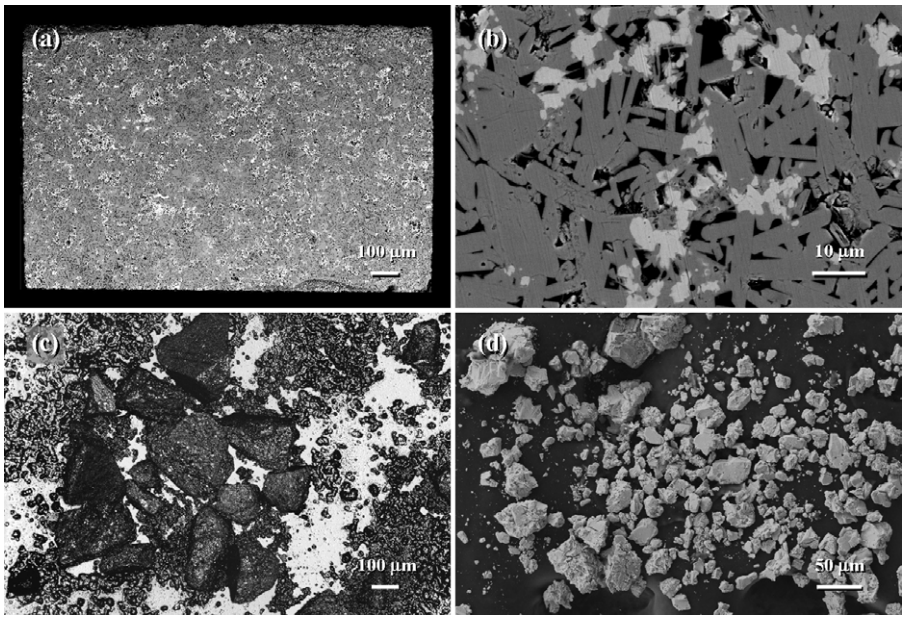

Figure 4. Scanning electron microscopy (SEM) images of the polished surface of $SmFeAsO_{0.85}$ ((a), (b)). Confocal laser scanning microscope image of the crushed pieces (c) and SEM image of the ground powder of $SmFeAsO_{0.85}$ (d).

measurement of the remanent moment, m_R [12, 20–22]. For a pure and homogeneous sample, we expect flux to penetrate when $H_a/(1-D)$ first exceeds the lower critical field B_{c1}, where D is the relevant demagnetizing factor. For weakly coupled polycrystals, where the weakness could occur either at grain boundaries or at non-superconducting second phases, flux penetration is expected to occur locally at lower fields than into the grains. Therefore information about the size of current loops derived from m_R (which is proportional to the product of J_c and current loop size) can be extracted from the dependence of m_R on the applied field H_a and the particle size. Accordingly, after measurement of each whole sample, we crushed them into tens of pieces and remeasured m_R, finally gently grinding the crushed pieces to powder in a mortar before remeasuring m_R. T_c did not change by crushing or powdering.

Figure 5(a) shows the remanent magnetization as a function of increasing applied field for the $SmFeAsO_{0.85}$ intact large bulk, a second, smaller bulk, the crushed pieces and ground powder. The m_R data are normalized by their respective sample masses of 30.0, 6.0, 14.2 and 4.3 mg. For the bulk samples, remanent magnetization began to increase on increasing the applied field above ∼5 mT, consistent with the reported B_{c1} of 5 mT for LaFeAs(O,F) [23], and a shoulder appeared at ∼80 mT in the m_R transition. This behavior is clearer in the derivative of $m_R(H_a)$ shown in figure 5(b) where two quite separate low-field peaks appear at 35 mT for the larger and at 18 mT for the smaller of the two bulk samples. By contrast, the second, higher field peak appeared at the same field of 150 mT for both samples. That the first peak strongly depends on sample size indicates that the bulk current loop is also size dependent, because the field of first penetration should be proportional to $H_p \sim J_c^{global} \times$ (sample size). This conclusion is strengthened by further suppression of the first peak in the crushed pieces and its disappearance almost to zero in the ground powder. In contrast, the second peak was found to be size independent, even after fine powdering, which means that the second peak is caused by locally circulating currents with current loop size less than the powder size of 20–50 μm.

Magneto-optical imaging (MOI) was performed to directly observe the local magnetic flux structure of the intact samples. Figure 6 shows MO images on a well polished surface of the $SmFeAsO_{0.85}$ bulk with a thickness of 440 μm. The light microscope image in figure 6(a) does not reveal any macroscale defects such as cracks or connected second phase fields that would block whole sample current flow. Under the zero-field-cooling (ZFC) condition we observe a bulk Meissner state when a field of 4 mT is applied at 6 K, as shown in figure 6(b), which indicates that the surface shielding current flows over the whole sample (magnetic domains in the MO imaging film are quite obvious too). As the external field increases, flux starts to penetrate at ∼6 mT and first reaches the center of the sample at ∼15 mT. However the MO images clearly show that flux penetration is quite inhomogeneous. As follows from figures 6(c) and (d), there are many 20–50 μm size black-appearing spots of strong flux shielding in the flux penetrated regions, indicative of local circulating currents with higher current density than the matrix. Similar electromagnetically granular behavior was also observed in the Nd bulk sample, as will be presented in figure 8. After the removal of the external field, the remanent trapped fields are shown in figures 6(e) and (f). These trapped fields were more homogeneous after applying a lower external field of 40 mT and, in contrast, many higher J_c spots (now white) appeared after applying 120 mT. These results are also consistent with the remanent magnetization data of figure 5(b), where the second peak appeared at 150 mT. Figures 6(g) and (h) show MO images under $\mu_0 H_{ex} = 0$ mT at $T = 6.4$ and 20 K, respectively, for the sample field-cooled in $\mu_0 H_{ex} = 120$ mT. It is particularly

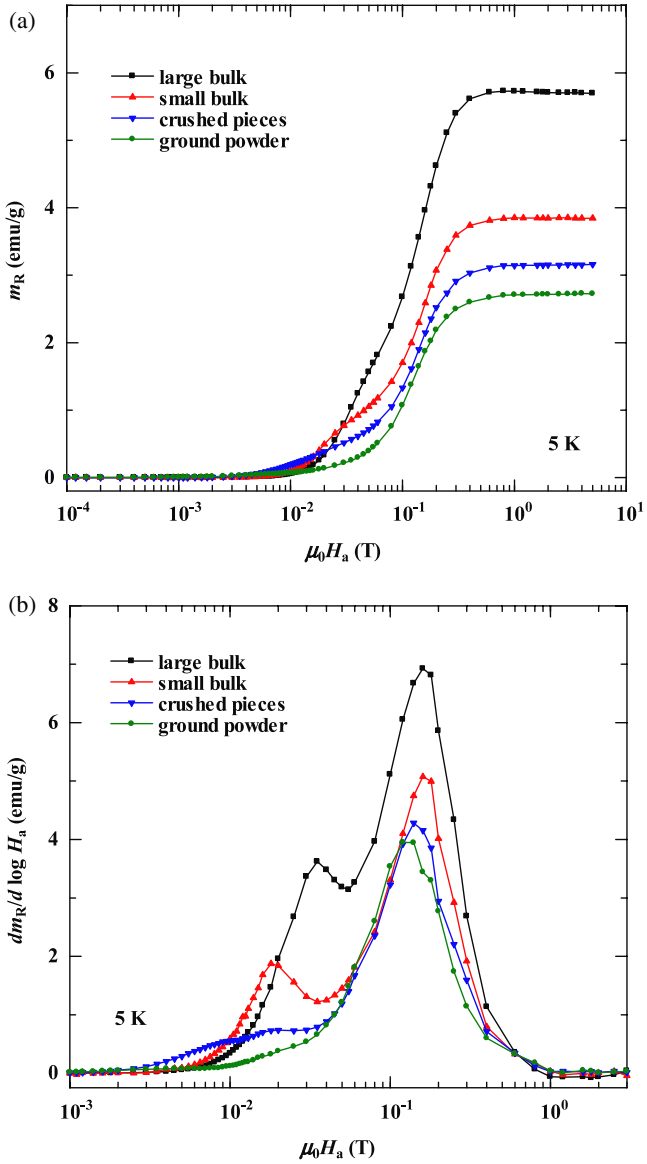

Figure 5. (a) Remanent magnetization (m_R) as a function of the maximum applied field at 5 K for the $SmFeAsO_{0.85}$ intact large bulk, intact small bulk, crushed pieces and ground powder. The data are normalized by the sample masses of 30.0, 6.0, 14.2 and 4.3 mg, respectively. (b) Derivatives of m_R at 5 K.

noteworthy that the strongly coupled local regions were clearly visible at 6.4 K, however, on raising the temperature to 20 K, a quasi-ideal, roof-top pattern then appears superimposed on the less visible granular structure. Therefore, the magnetic granularity is more pronounced below 15 K and becomes progressively less visible at higher temperatures. Field-cooled MO contrast of the roof-top pattern of the trapped flux state was visible up to 48 K, indicating persistent bulk currents up to almost 90% of $T_c \sim 54$ K.

This temperature-dependent granular behavior is quite prominent in flux density profiles. Figure 7 shows magnetic flux profiles $B(x)$ taken at (a) 6.4 K and (b) 20 K for the Sm sample field-cooled under $\mu_0 H_{ex} = 120$ mT. The profiles are taken along the same line (line 1) as indicated by arrows in figure 6(g) and (h), respectively. A bulk scale critical state with global J_c of 2.0×10^3A cm^{-2} at 20 K was deduced from this flux gradient, but the gradients are indeed strongly perturbed at 6 K by the local domains, which correspond directly to the white spots in figure 6.

Figure 8 shows MO images taken on the polished surface of the $NdFeAsO_{0.94}F_{0.06}$ bulk. Topographic light microscopy images (figure 8(a)) shows dark-appearing impurity phases 100–300 μm in size and light-appearing particles, which were identified to be Fe–As glassy phase and Nd_2O_3 particles by EDS analyses. Figures 8(b)–(d) show the MO images of the sample after zero-field cooling to 6 K. Figure 8(b) shows that flux penetrates preferentially through the larger impurity phases and reaches the center of the sample under an external field of 40 mT. Granular behavior was also observed after applying a higher magnetic field of 120 mT, as shown in figure 8(e). The 10–20 μm size of the strongly connected white spots was smaller than those of the Sm sample, consistent with our observation that the ~5 μm grain size of the Nd sample is about half that of the Sm sample. Magnetic flux profiles $B_z(x)$ taken along line 2 in figure 8(a) are shown in figure 9, where it is also seen that a bulk critical state is quite visible at 20 K, but that more inhomogeneous behavior is observed at 6.2 K.

Figure 10 shows the derivative of $m_R(H_a)$ for the $SmFeAsO_{0.85}$ bulk at 5, 10, 15, 20, 30 and 40 K, while the inset figure shows the temperature dependence of the first and second peaks in the derivative of the $m_R(H_a)$ plots. The second high-field peak shows a strong temperature dependence and a marked shift towards higher fields below ~15 K, indicative either of a strongly increasing local critical current density or/and a growing current loop size. On the other hand, the low-field global current peak showed a much weaker temperature dependence. These quite different temperature dependences result in a merging of the two peaks at temperatures above 15 K, as is consistent with the MO images seen in figure 6.

Figure 11 shows the derivative of $m_R(H_a)$ for the $NdFeAsO_{0.94}F_{0.06}$ bulk sample at 5, 10, 20, 30 and 35 K. Similar to the Sm sample, the second peak shifts rapidly as the temperature decreases. A third peak (~110 mT) appeared at 5 K. Since the ratio of the fields of the second and third peaks is ~4, and this value is comparable to the square root of the resistivity anisotropy ratio ~15 [24], the peak split might be due to an anisotropic J_c. The inset to figure 11 shows the temperature dependence of the first, second and third peaks. As for the Nd sample, the temperature dependence of the second and third peaks was strong below ~10 K. A minor peak was observed at ~300 mT and was almost temperature independent. This peak at 200–300 mT was also observed in the Sm and $LaFeAsO_{0.89}F_{0.11}$ samples. It might have its origin in a minority paramagnetic phase and is not further discussed in this paper.

Global and local J_c values for the Sm and Nd bulk samples were calculated independently from the peak positions in the derivative of $m_R(H_a)$. For the J_c calculation we assumed a thin plate in parallel field for the bulk current and spherical grains for the local current. By neglecting the demagnetization factor and anisotropy of J_c, both of which are unknown at this stage of oxypnictide studies, the Bean model shows that the global and local J_c can be given as $J_c^{global} = 2H_{peak1}/w$

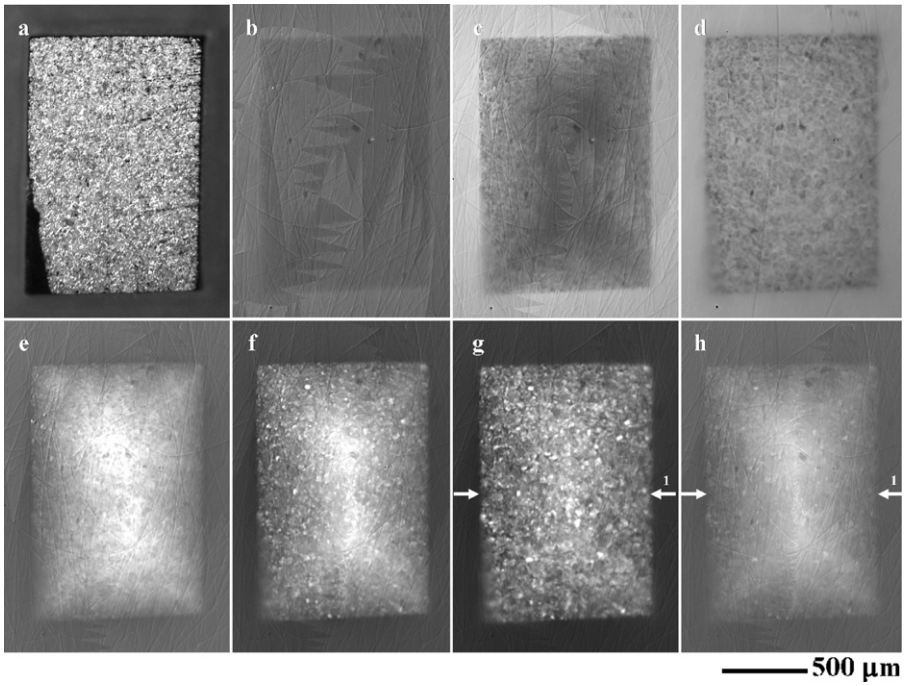

Figure 6. Magneto-optical images taken on the $SmFeAsO_{0.85}$ bulk sample. (a) Light microscopy image of a polished surface of the $SmFeAsO_{0.85}$ bulk. ((b)–(f)) MO images of different stages of magnetic flux penetration into the sample for ZFC at (b) $T = 6$ K and $\mu_0 H_{ex} = 4$ mT, (c) $\mu_0 H_{ex} = 12$ mT, (d) $\mu_0 H_{ex} = 120$ mT, (e) $\mu_0 H_{ex} = 0$ mT after applying 40 mT, (f) $\mu_0 H_{ex} = 0$ mT after applying 120 mT. ((g), (h)) MO images under $\mu_0 H_{ex} = 0$ mT at (g) $T = 6.4$ K and (h) 20 K field cooling (FC) in $\mu_0 H_{ex} = 120$ mT. Arrows shown in (g) and (h) indicate line 1 for magnetic flux profiles shown in figure 7.

and $J_c^{local} = 2.81 H_{peak2}/r$, where w is the thickness of the whole, bulk sample and r is the grain radius. From microstructural analyses, grain sizes were estimated to be 10 μm for the Sm sample and 5 μm for the Nd sample, leading to the global and local J_c as a function of temperature shown in figures 12 and 13, respectively. Global J_c values were also calculated from MO flux profiles and these values are also shown in figure 12, as is J_c calculated from the width of the flux penetration front in the ZFC image using formulas in [17, 18, 25]. The agreement on J_c between these various methods of extracting the global J_c is excellent. The temperature dependence of the global J_c is almost linear, except near T_c, and J_c values at 5 K of 3900 and 2100 A cm^{-2} for the Sm and Nd samples, respectively, are obtained.

The temperature dependence of the local J_c, for currents circulating only within individual grains, is shown in figure 13. The J_c values are 4.5×10^6 and 6.7×10^6 A cm^{-2} at 5 K for the Sm and Nd samples, respectively. These values are considerably higher than those recently deduced by Prozorov *et al* (3×10^5 A cm^{-2} [13]), by Senatore *et al* (6×10^4 A cm^{-2} for 10 μm grain size and 6×10^6 A cm^{-2} for 0.1 μm [14]) and by Wang *et al* (2×10^5 A cm^{-2} [26]). Both Sm and Nd samples showed strong upward curvature in $J_c(T)$ below ~20 K.

Finally we plot the ratio of the global and local, that is the deduced intragrain J_c values in figure 14. The ratio $J_c^{global}(T)/J_c^{local}(T)$ increases as temperature decreases, reaches a maximum at ~25 K and drops rapidly at low temperatures. The ratio never exceeds 0.004 and falls to ~0.001 at ~5 K when the electromagnetically granular behavior revealed by the MO imaging and remanent field analysis becomes so marked.

4. Discussion

The sample-size-dependent remanent magnetization showed that two (or even three in the case of the Nd sample) distinct scales of current flow exist in these iron oxypnictide samples. The spatial variation of the scales is directly demonstrated by MO imaging where obvious spots of higher J_c appear in a lower J_c matrix in field-cooled images. Here we discuss the origins of this electromagnetically granular behavior, especially the issue of whether the granularity is intrinsic or extrinsic to these samples.

We start discussion with the scales of the global and local currents. The strong sample size dependence of the first peak of the remanent magnetization shown in figure 5(b) strongly suggests that a global current does circulate over the whole sample. This is in strong contrast to the previously reported data on a $LaFeAsO_{0.89}F_{0.11}$ sample where almost no bulk current was observed and only one, size-independent (equivalent to the second peak in the present data) peak appeared in the remanent magnetization [12]. Like the La sample data, the size independence of this second peak in figure 5(b) shows that the local current loop size is less than the powder size of ~50 μm shown in figure 4(d). Independent evidence of the scale of the locally high J_c domains is provided by the white spots with size of 10–50 μm in the MO images shown in figure 6(g). We therefore conclude that a significant fraction of the local current loops are on the scale of the grain size, which lies principally in the 5–10 μm range.

An important scientific and technological issue is whether the substantial restriction of strong current density within the grains of this untextured, or very weakly textured

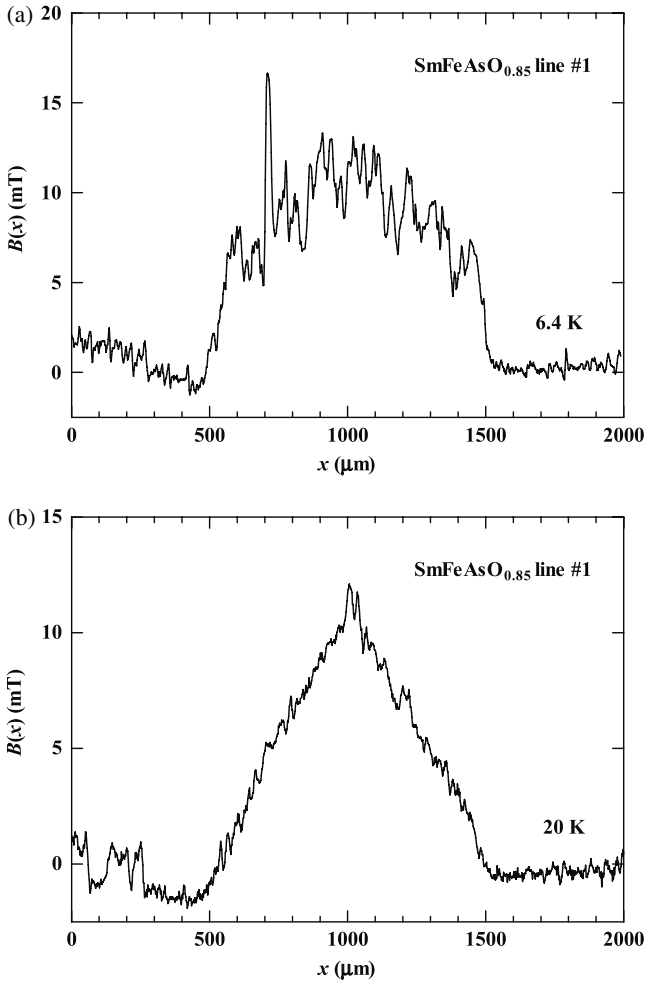

Figure 7. Magnetic flux profiles $B_z(x)$ taken at (a) 6.4 K and (b) 20 K along the line 1 in figures 6(g) and (h), respectively. The sample was field-cooled under $\mu_0 H_{ex} = 120$ mT down to 6 K followed by removal of the external field, and then the temperature was increased.

sample (unpublished EBSD shows few signs of low-angle grain boundaries in the samples [27]) is intrinsic to the oxypnictides or due to extrinsic features of these particular samples. So far as the possibility of intrinsic granularity is concerned, one important factor is likely to be the low carrier density of $\sim 10^{21}$ cm^{-3} [4] which is very similar to that found in the cuprates, where it contributes significantly to an intrinsic weak-link behavior at high-angle cuprate grain boundaries [28, 29]. However, many additional specific features of the cuprates, including their sensitivity to local oxygen concentration, proximity of the superconducting state to the Mott metal–insulator transition, and cation disorder [30], also play important roles in depressing the superconducting order parameter at grain boundaries. Explicit understanding of the oxypnictides awaits single grain-boundary studies that are not yet possible, so for now we restrict our discussion to extrinsic factors that may be playing a role in the behavior of these two Nd and Sm samples, that actually show much better global current flow than the La oxypnictide sample first studied [12].

First it is clear from the MO images of figure 8(b) that the macroscale impurity phases (principally RE_2O_3 and the glassy Fe–As phase) shown in figures 4(b) and 8(a) do allow flux to easily penetrate the Nd sample. It is also seen that the global J_c of the Nd sample is less than the Sm sample which has fewer second phases, a correlation that does suggest that macroscale impurities limit the global current, in analogy to the case of porous, polycrystalline MgB_2 where voids and impurity insulating MgO significantly reduce percolating current paths and limit the normal-state conductivity and critical current density [31, 32]. Considering the very different length scales of superconducting coherence length (<5 nm) and these impurities (several tens to several hundreds of microns), the macroscale secondary phases are more likely to block global current flow, rather than to contribute to vortex pinning.

Second it is possible that many superconducting grains are isolated from each other by non-superconducting layers, particularly the grain-boundary wetting, Fe–As amorphous phase. A TEM study in progress does show that some grain boundaries are covered by such wetting phases with a thickness of several tens of nanometers, although some clean grain boundaries are also observed [27]. Depending on the thickness and properties of the wetting phase, such layers might act as barriers that completely decouple the grains or act as weakly coupled Josephson junctions with rather different temperature- and field-dependent critical current density compared to the vortex pinning current density circulating within grains. Indeed the strong temperature dependence of $J_c^{global}(T)/J_c^{local}(T)$ in figure 14 shows very clearly that two different mechanisms control the inter and intragranular current densities. The temperature dependence of the global J_c near T_c with upward curvature is found to be well fitted by a quadratic function $J_c \propto (T_c - T)^2$ suggestive of an SNS proximity coupled Josephson junction [33, 34] which has also been observed on low-angle grain boundaries in cuprate superconductors [35, 36]. Therefore we may conclude that the intergranular current transport in the present samples is limited by the proximity coupled conductive wetting glassy As–Fe phase or by the intrinsic weak coupling. H_{c2} measurements on these two samples suggest that $H_{c2}(0)$ is well over 100 T, making the coherence length shorter than 2 nm, thus adding weight to the concern that there is an intrinsic aspect to the limitation of current across high-angle grain boundaries. The already noted negligible global current observed in the $LaFeAsO_{0.89}F_{0.11}$ sample surprised us due to its relatively low normal-state resistivity ($\sim$0.15 mΩ cm) and high RRR of 15 ($\sim$3 for the present samples), both factors which might suggest higher intergranular J_c behavior for the $LaFeAsO_{0.89}F_{0.11}$ sample. However, the measured normal-state resistivity at T_c ($\sim$0.5 mΩ cm) of the Sm and Nd samples may be significantly overestimated if the second phase content forces strong current percolation. This would of course be fully consistent with a suppressed $J_c^{global}(T)/J_c^{local}(T)$. We therefore conclude that our present data are insufficient to decide on the balance between intrinsic and extrinsic limitation of J_c in the present samples and that there is evidence to support both mechanisms.

Another point to address is the comparative behavior of the polycrystalline oxypnictides to randomly oriented

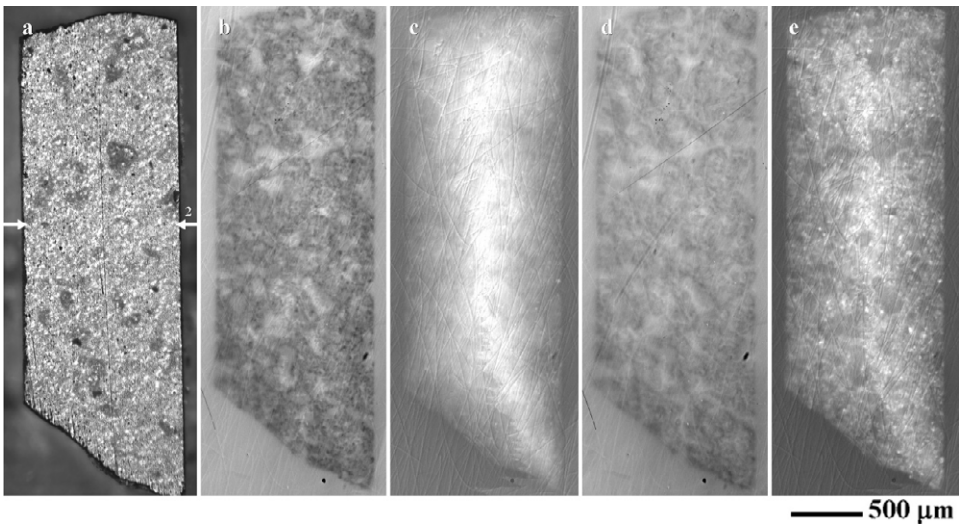

Figure 8. Magneto-optical images taken on the polished surface of the $NdFeAsO_{0.94}F_{0.06}$ bulk sample. (a) Surface image by optical microscopy. MO images of different stages of magnetic flux penetration into the sample for ZFC to $T = 6$ K and (b) after application of $\mu_0 H_{ex} = 40$ mT, (c) then reducing the field $\mu_0 H_{ex} = 0$ mT, (d) then after applying $\mu_0 H_{ex} = 120$ mT, (e) and finally after reducing $\mu_0 H_{ex} = 0$ mT. An arrow shown in (a) indicates line 2 for magnetic flux profiles shown in figure 9.

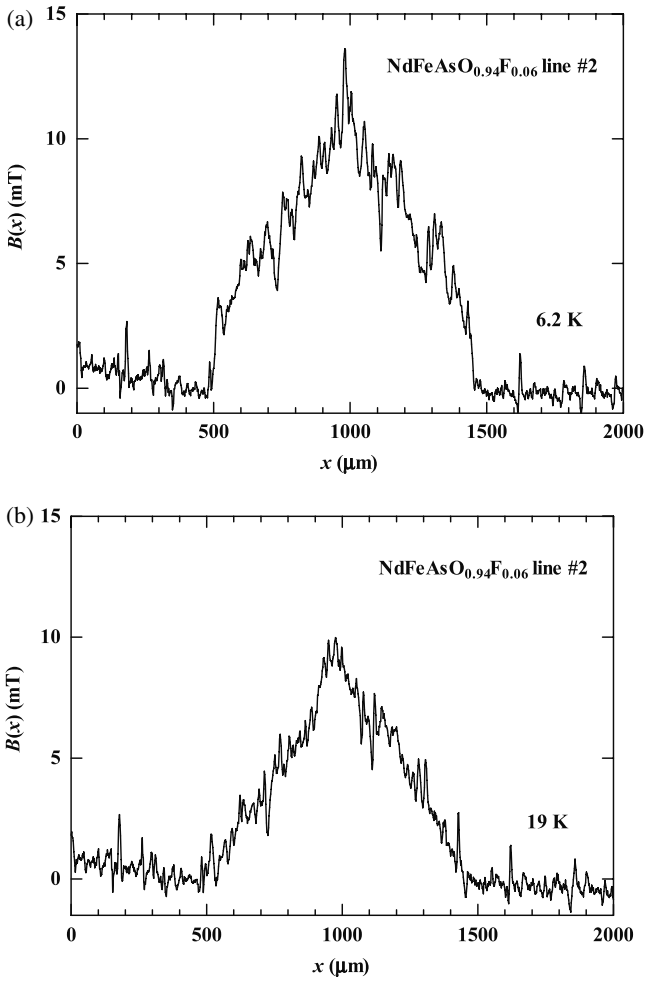

Figure 9. Magnetic flux profiles $B_z(x)$ taken along line 2 in figure 8(a) at (a) 6.2 K and (b) 19 K. The sample was field-cooled under $\mu_0 H_{ex} = 120$ mT down to 6 K followed by removal of the external field and increase of temperature to 19 K.

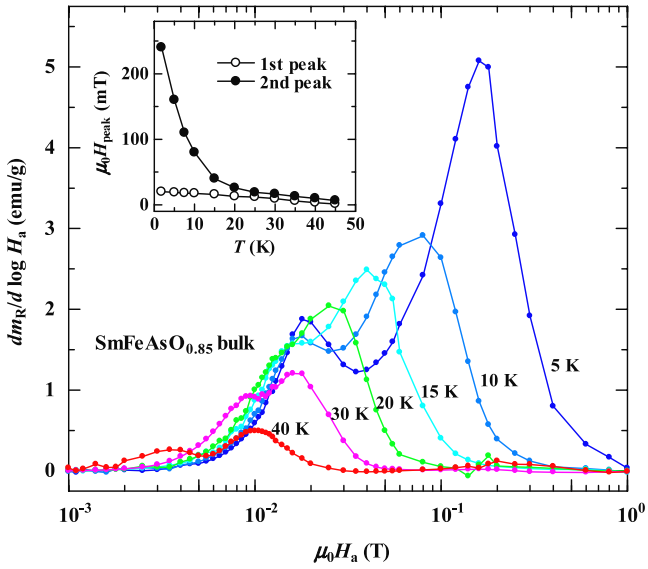

Figure 10. Derivatives of the remanent magnetization as a function of the maximum applied field for the $SmFeAsO_{0.85}$ small bulk. Data are normalized by sample mass. Inset shows the temperature dependences of the peak fields $\mu_0 H_{peak}$ for the first and second peaks.

polycrystalline MgB_2 and cuprates. The global J_c values of 4000 and 2000 A cm^{-2} at 5 K obtained for the Sm and Nd samples is significantly lower than those seen in random bulks of MgB_2 which generally attain 10^6A cm^{-2} at 4 K [37, 38]. However, it was very early established that grain boundaries were not intrinsic obstacles to current flow in MgB_2 [39]. Of greater interest is the comparison to the least anisotropic of the cuprates, those with the RE-123 structure, randomly oriented polycrystalline examples of which have global J_c values of only ∼100 A cm^{-2} at 4 K due to large intrinsic

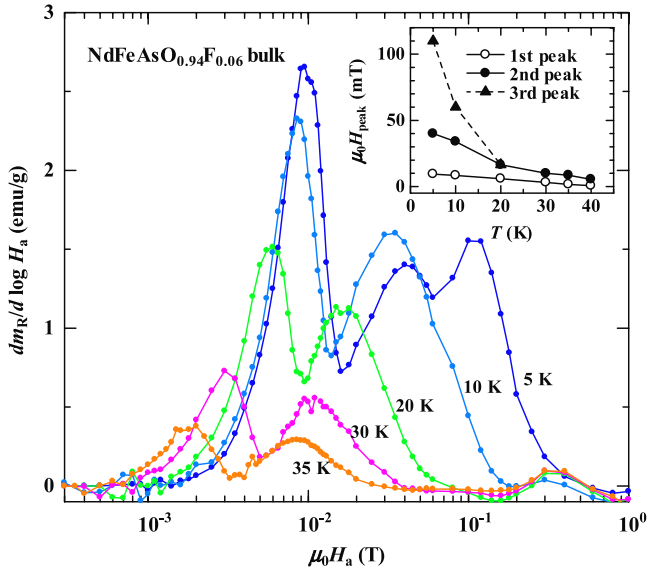

Figure 11. Derivatives of remanent magnetization as a function of the maximum applied field for the $NdFeAsO_{0.94}F_{0.06}$ bulk sample. Data are normalized by sample mass. Inset shows the temperature dependences of the peak fields $\mu_0 H_{peak}$ for the first, second and third peaks.

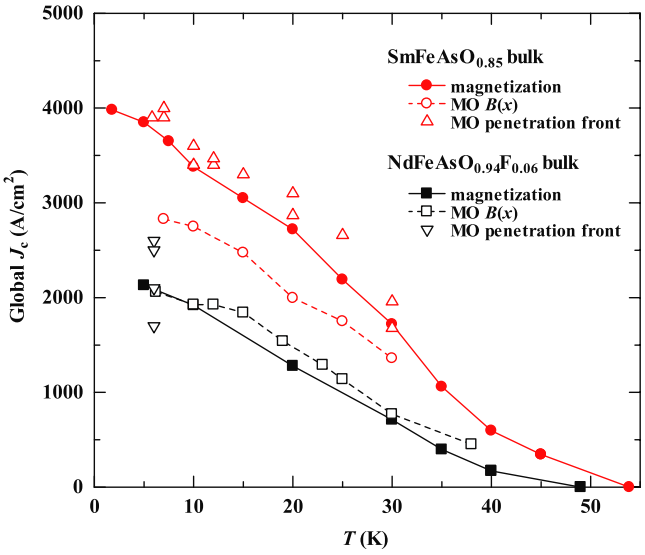

Figure 12. Temperature dependence of global critical current density $J_c^{global}(T)$ for $SmFeAsO_{0.85}$ and $NdFeAsO_{0.94}F_{0.06}$ bulk samples obtained from the remanent magnetization analysis (filled), magneto-optical $B(x)$ flux profile analysis for the FC conditions, and the width of the flux penetration front in the ZFC conditions using Brandt's expression [21] for a strip in perpendicular field.

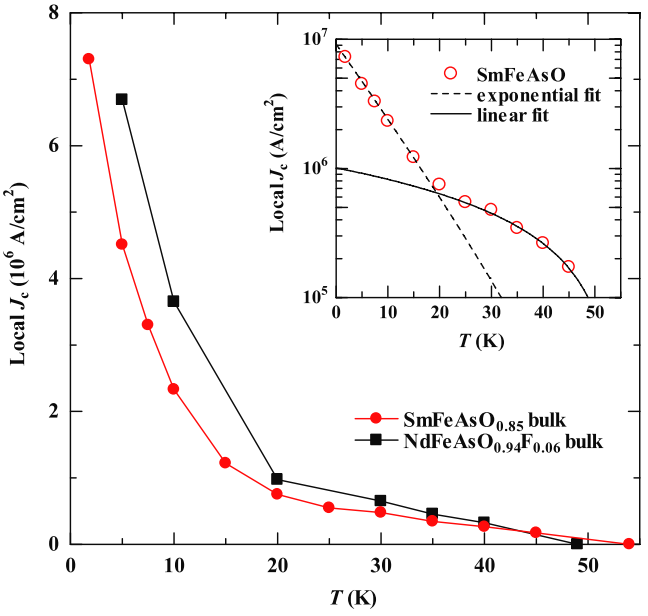

Figure 13. Temperature dependence of critical current density of locally circulating current $J_c^{local}(T)$ for $SmFeAsO_{0.85}$ and $NdFeAsO_{0.94}F_{0.06}$ bulk samples obtained from remanent magnetization analysis. Inset shows log-scale plots for the $SmFeAsO_{0.85}$ data with exponential and linear fitting.

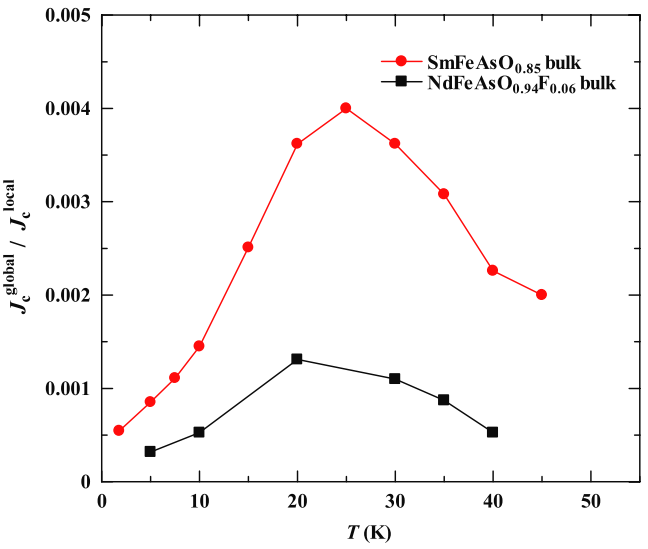

Figure 14. Temperature dependence of the ratio $J_c^{global}(T)/J_c^{local}(T)$ for the $SmFeAsO_{0.85}$ and $NdFeAsO_{0.94}F_{0.06}$ bulk samples.

weak-link effects [15, 16]. Thus it may be that any intrinsic weak-link effect at oxypnictide grain boundaries is less serious than in the cuprates. The lower H_{c2} anisotropy γ and higher carrier density in the iron oxypnictides ($\gamma \sim 4$) compared to the cuprates such as YBCO ($\gamma \sim 7$) could be the reasons for the higher bulk J_c in the randomly oriented Sm and Nd polycrystalline samples.

Finally, the temperature dependence of local J_c is briefly discussed. A rather linear temperature dependence of local J_c is observed near T_c for both the Sm and Nd samples, as shown in the inset to figure 13. This temperature dependence, very high $J_c(0) \sim 8 \times 10^6$ A cm^{-2} and a wide magnetization hysteresis loop indicate that strong intragrain vortex pinning is present in these samples. On the other hand, an upward curvature in $J_c(T)$ is observed below ~20 K and $J_c(T)$ decreases rapidly with increasing temperature. This behavior may indicate significant thermal fluctuation of vortices, which result in a similar upturn of $J_c(T)$ at low temperature in the cuprate single crystals [17]. The $J_c(T)$ curves at low temperature can be fitted by an exponential function as shown in the inset to figure 13 using

an equation $J_c = A(1 - T/T_c)\exp(-T/T_0)$, with $T_0 = 8$–10 K. The exponential factor can be understood using the following simple model. Vortex fluctuations smear out the pinning potential, reducing the elementary pinning forces by the Debye–Waller factor $\exp(-\langle u^2\rangle/a^2)$ where u is the thermal displacement of a vortex from the pinning well of size a [40]. Then from the equipartition theorem $G\langle u^2\rangle = k_B T$, we obtain $\exp(-\langle u^2\rangle/a^2) = \exp(-T/T_0)$. Here the depinning temperature $T_0 = Ga^2/k_B$, depends on the size of pinning centers a, and the Campbell pinning spring constant G. A crossover of the linear and exponential behaviors occurred at ∼20 K as shown in the inset to the figure 13, indicating that thermal fluctuations provoke the rapid decrease of the local J_c at high temperatures. The deduced depinning temperature $T_0 = 8.8$ K turns out to be rather low compared to $T_c = 54$ K, indicating either that the size of vortex pinning centers is small or the spring constant is small, perhaps due to strong anisotropy of these sample. Noteworthy too is the fact that although the nominal doping level of the $SmFeAsO_{0.85}$ ($x = 0.15$ oxygen deficiency) and $NdFeAsO_{0.94}F_{0.06}$ ($x = 0.06$ fluorine doping) samples are quite different, the deduced temperature dependence of the local J_c is quite similar, indicating either that the actual doping states differ from the nominal composition and/or that vortex pinning is less sensitive to RE type and doping level than in the cuprates.

5. Summary

Two distinct scales of current flow in the polycrystalline $SmFeAsO_{0.85}$ and $NdFeAsO_{0.94}F_{0.06}$ samples were quantitatively evaluated by remanent magnetization measurements and local magneto-optical imaging. A strong sample size-dependent remanent magnetization characteristic was found; however, independent MO observations of the Bean critical state over the whole sample showed that a global current can exist in iron oxypnictides with J_c of the order of ∼4000 A cm^{-2} at 5 K and self-field. The temperature dependence of the global and local J_c was independently derived from the penetration fields obtained from the global magnetization measurements and it was found that the two currents had quite different temperature dependences and that their ratio $J_c^{global}(T)/J_c^{local}(T)$ never exceeded ∼0.004. An SNS proximity coupled intergranular current was suggested from the temperature dependence of global J_c. The local J_c value at self-field and 5 K is estimated to be $\sim 5 \times 10^6$ A cm^{-2}. Temperature dependence of local J_c showed strong upturn below 15 K which is similar to the cuprate superconductors. Similar to the cuprates, we also found evidence for electromagnetic granularity, though with not quite so much reduction of J_c in polycrystalline bulks. To fully understand the balance of intrinsic and extrinsic factors, study of individual grain boundaries of known misorientations will be very helpful.

Acknowledgments

Work at the NHMFL was supported by IHRP 227000-520-003597-5063 under NSF Cooperative Agreement DMR-0084173, by the State of Florida, by the DOE, by the NSF Focused Research Group on Magnesium Diboride (FRG) DMR-0514592 and by AFOSR under grant FA9550-06-1-0474. One of the authors (AY) is supported by a fellowship of the Japan Society for the Promotion of Science.

References

[1] Kamihara Y, Watanabe T, Hirano M and Hosono H 2008 Iron-based layered superconductor La[$O_{1-x}F_x$]FeAs ($x = 0.05$–0.12) with $T_c = 26$ K *J. Am. Chem. Soc.* **130** 3296

[2] Day C 2008 New family of quaternary iron-based compounds superconducts at tens of kelvin *Phys. Today* **61** 11

[3] Takahashi H, Igawa K, Arii K, Kamihara Y, Hirano M and Hosono H 2008 Superconductivity at 43 K in an iron-based layered compound $LaO_{1-x}F_xFeAs$ *Nature* **453** 376

[4] Sefat A S, McGuire M A, Sales B C, Jin R, Howe J Y and Mandrus D 2008 Electronic correlations in the superconductor $LaFeAsO_{0.89}F_{0.11}$ with low carrier density *Phys. Rev.* B **77** 174503 (*Preprint* 0803.2528v1 [cond-mat])

[5] Chen G F, Li Z, Wu D, Li G, Hu W Z, Dong J, Zheng P, Luo J L and Wang N L 2008 Superconductivity at 41 K and its competition with spin-density-wave instability in layered $CeO_{1-x}F_xFeAs$ *Preprint* 0803.3790v1 [cond-mat]

[6] Hunte F, Jaroszynski J, Gurevich A, Larbalestier D C, Jin R, Sefat A S, McGuire M A, Sales B C, Christen D K and Mandrus D 2008 Very high field two-band superconductivity in $LaFeAsO_{0.89}F_{0.11}$ *Nature* **453** 903
(Hunte F, Jaroszynski J, Gurevich A, Larbalestier D C, Jin R, Sefat A S, McGuire M A, Sales B C, Christen D K and Mandrus D 2008 *Preprint* 0804.0485v1 [cond-mat])

[7] Chen X H, Wu T, Wu G, Liu R H, Chen H and Fang D F 2008 Superconductivity at 43K in Samarium-arsenide Oxides $SmFeAsO_{1-x}F_x$ *Nature* **453** 761
(Chen X H, Wu T, Wu G, Liu R H, Chen H and Fang D F 2008 *Preprint* 0803.3603v1 [cond-mat])

[8] Ren Z A *et al* 2008 Superconductivity in iron-based F-doped layered quaternary compound Nd[$O_{1-x}F_x$]FeAs *Europhys. Lett.* **82** 57002 (*Preprint* 0803.4234v1 [cond-mat])

[9] Ren Z A, Yang J, Lu W, Yi W, Che G C, Dong X L, Sun L L and Zhao Z X 2008 Superconductivity at 52 K in iron-based F-doped layered quaternary compound Pr[$O_{1-x}F_x$]FeAs *Preprint* 0803.4283v1 [cond-mat]

[10] Ren Z A *et al* 2008 Superconductivity at 55 K in iron-based F-doped layered quaternary compound Sm[$O_{1-x}F_x$]FeAs *Chin. Phys. Lett.* **25** 2215 (*Preprint* 0804.2053v1 [cond-mat])

[11] Yang J *et al* 2008 Superconductivity at 53.5 K in $GdFeAsO_{1-\delta}$ *Supercond. Sci. Technol.* **21** 082001 (*Preprint* 0804.3727v1 [cond-mat])

[12] Yamamoto A *et al* 2008 Evidence for electromagnetic granularity in the polycrystalline iron-based superconductor $LaO_{0.89}F_{0.11}FeAs$ *Appl. Phys. Lett.* **92** 252501
(Yamamoto A *et al* 2008 *Preprint* 0805.1282v1 [cond-mat])

[13] Senatore C, Wu G, Liu R H, Chen X H and Flukiger R 2008 Upper critical fields well above 100 T for the superconductor $SmO_{0.85}F_{0.15}FeAs$ with $T_c = 46$ K *Preprint* 0805.2389v1 [cond-mat]

[14] Prozorov R, Tillman M E, Mun E D and Canfield P C 2008 Intrinsic magnetic properties of $Nd(O_{0.9}F_{0.1})FeAs$ superconductor from local and global measurements *Preprint* 0805.2783v1 [cond-mat]

[15] Larbalestier D C *et al* 1987 Experiments concerning the connective nature of superconductivity in $YBa_2Cu_3O_7$ *J. Appl. Phys.* **62** 3308

[16] Seuntjens J M and Larbalestier D C 1990 On the improvement of $DyBa_2Cu_3O_{7-\delta}$ properties through better sintering *J. Appl. Phys.* **67** 2007

[17] Polyanskii A A, Gurevich A, Pashitski A E, Heinig N F, Redwing R D, Nordman J E and Larbalestier D C 1996 Magneto-optical study of flux penetration and critical current densities in [001] tilt $YBa_2Cu_3O_{7-\delta}$ thin-film bicrystals *Phys. Rev.* B **53** 8687

[18] Polyanskii A A, Feldmann D M and Larbalestier D C 2003 Magneto-Optical characterization techniques *Handbook of Superconducting Materials* ed D Cardwell (Bristol: IOP Publishing) chapter D3.4, pp 1551–67 University of Cambridge, UK; D. Ginley, NREL

[19] Tarantini C, Gurevich A, Larbalestier D C, Ren Z A, Dong X L, Lu W and Zhao Z X 2008 Can antiferromagnetism and superconductivity coexist in the high-field paramagnetic superconductor Nd(O, F)FeAs? *Preprint* 0805.4445v1 [cond-mat]

[20] Muller K H, Andrikidis C, Liu H K and Dou S X 1994 Intergranular and intragranular critical currents in silver-sheathed Pb–Bi–Sr–Ca–Cu–O tapes *Phys. Rev.* B **50** 10218

[21] Muller K H, Andrikidis C, Du J, Leslie K E and Foley C P 1999 Connectivity and limitation of critical current in Bi–Pb–Sr–Ca–Cu/Ag tapes *Phys. Rev.* B **60** 659

[22] Polyanskii A, Feldmann D M, Patnaik S, Jiang J, Cai X, Larbalestier D, DeMoranville K, Yu D and Parrella R 2001 Examination of current limiting mechanisms in monocore $Bi_2Sr_2Ca_2Cu_3O_x$ tape with high critical current density *IEEE Trans. Appl. Supercond.* **11** 3269

[23] Ren C, Wang Z S, Yang H, Zhu X, Fang L, Mu G, Shan L H and Wen H 2008 Linear temperature dependence of the lower critical field H_{c1} in F-Doped LaOFeAs Superconductors *Preprint* 0804.1726v1 [cond-mat]

[24] Singh D J and Du M H 2008 $LaFeAsO_{1-x}F_x$: a low carrier density superconductor near itinerant magnetism *Preprint* 0803.0429v1 [cond-mat]

[25] Brandt E H and Indenbom M 1993 Type-II-superconductor strip with current in a perpendicular magnetic field *Phys. Rev.* B **48** 12893

[26] Wang X L, Ghorbani R, Peleckis G and Dou S X 2008 Very high critical field and superior J_c-field performance in $NdO_{0.82}F_{0.18}FeAs$ with T_c of 51 K *Preprint* 0806.0816v1 [cond-mat]

[27] Kametani F *et al* 2008 to be submitted to *Supercond. Sci. Technol.*

[28] Dimos D, Chaudhari P, Mannhart J and LeGoues F K 1988 Orientation dependence of grain-boundary critical currents in $YBa_2Cu_3O_{7-\delta}$ bicrystals *Phys. Rev. Lett.* **61** 219

[29] Larbalestier D, Gurevich A, Feldmann D M and Polyanskii A 2001 High-T_c superconducting materials for electric power applications *Nature* **414** 368

[30] Song X Y, Daniels G, Feldmann D M, Gurevich A and Larbalestier D 2005 Electromagnetic, atomic structure and chemistry changes induced by Ca-doping of low-angle $YBa_2Cu_3O_{7-\delta}$ grain boundaries *Nat. Mater.* **4** 470

[31] Rowell J M 2003 The widely variable resistivity of MgB_2 samples *Supercond. Sci. Technol.* **16** R17

[32] Yamamoto A, Shimoyama J, Kishio K and Matsushita T 2007 Limiting factors of normal-state conductivity in superconducting MgB_2: an application of mean-field theory for a site percolation problem *Supercond. Sci. Technol.* **21** 658

[33] de Gennes P G 1964 Boundary effects in superconductors *Rev. Mod. Phys.* **36** 225

[34] Golubov A A, Kupriyanov M Yu and Il'ichev E 2004 The current-phase relation in Josephson junctions *Rev. Mod. Phys.* **76** 411

[35] Darhmaoui H and Jung J 1996 Crossover effects in the temperature dependence of the critical current in $YBa_2Cu_3O_{7-\delta}$ *Phys. Rev.* B **53** 14621

[36] Gurevich A, Rzchowski M S, Daniels G, Patnaik S, Hinaus B M, Carillo F, Tafuri F and Larbalestier D C 2002 Flux flow of Abrikosov–Josephson vortices along grain boundaries in high-temperature superconductors *Phys. Rev. Lett.* **88** 097001

[37] Flukiger R, Suo H L, Musolino N, Beneduce C, Toulemonde P and Lezza P 2003 Superconducting properties of MgB_2 tapes and wires *Physica* C **385** 286

[38] Senkowicz B J, Polyanskii A, Mungall R J, Zhu Y, Giencke J E, Voyles P M, Eom C B, Hellstrom E E and Larbalestier D C 2007 Understanding the route to high critical current density in mechanically alloyed $Mg(B_{1-x}C_x)_2$ *Supercond. Sci. Technol.* **20** 650

[39] Larbalestier D C *et al* 2001 Strongly linked current flow in polycrystalline forms of the superconductor MgB_2 *Nature* **410** 186

[40] Blatter G, Feigel'man M V, Geshkenbein V B, Larkin A I and Vinokur V M 1994 Vortices in high-temperature superconductors *Rev. Mod. Phys.* **66** 1125